2024 46th Annual International Conference of the IEEE Engineering in Medicine and Biology Society (EMBC) | 979-8-3503-7149-9/24/$31.00 ©2024 IEEE | DOI: 10.1109/EMBC53108.2024.10781921

Bedside Admittance Control of a Dual-Segment Soft Robot for Catheter-Based Interventions

Noah Barnes[1], Shaopeng Jiang[2], Lingyun Di[2], Hannah Qu[3], Miroslaw Janowski[4], Charles I. Berul[5], Adira Colton[6], Olivia Young[6], Ryan D. Sochol[6], Jeremy D. Brown[1], and Axel Krieger[1]

***Abstract*—Robotic catheters enable precise steering of their distal tip while inside the body's blood vessels, and with this ability comes the need for control systems that fit into the clinical workflow. In this study, we propose a novel bedside admittance controller composed of a force/torque sensor with a 3D-printed handle and a low-profile table mount. The controller is intended to be placed at the insertion site to the body and allows simultaneous insertion and steering of a dual-segment fluid-actuated soft robot catheter. This teleoperated system is characterized and evaluated in a simulated cardiac ablation task using a two dimensional 3D-printed atrium-like cavity. Four novices controlled the soft robot catheter with an average position error of 0.4 mm and angle error of 4.6 degrees, as compared to position error of 1.0 mm and angle error of 18.2 degrees attained by an expert cardiologist using a standard ablation catheter. The controller enables intuitive control of a dual channel soft robot and the preliminary results indicate the potential advantage of such an approach in catheter-based interventions with increasingly complex catheter robots.**

***Index Terms*—robotic catheter, admittance control, soft robot**

I. Introduction

In endovascular procedures, catheters are inserted into the body to diagnose and treat various vascular diseases. Robotic catheters may help overcome the navigation and control challenges of nonrobotic catheters by increasing their available degrees-of-freedom (DoFs) [1], [2]. To effectively make use of the added functionality, it is important to develop control interfaces that fit within the clinical workflow. The simplest controllers utilize mechanical interfaces at the proximal end of the instrument [3]–[5], however they can require high forces to actuate, suffer from mechanical complexity, and do not provide an opportunity for assistive or closed-loop control using an external computer. Conversely, there exist many remote teleoperated systems [6]–[12], however they necessitate complex control infrastructures which generally omit the haptic feedback experienced during manual operation, and often still require a member of the operating team to be bedside to manage the follower robot [13].

Given the trade-off that exists between manual and fully remote control, a desirable compromise is bedside robotic controllers, which preserve the ability to achieve low physical exertion and closed-loop control without the need for complex external control infrastructure [14]. Such systems have demonstrated utility in other clinical applications, and can largely be separated into grounded [15] and ungrounded (or handheld) [16], [17] systems. Grounded bedside robotic controllers transmit force between the robot and operator through an interface that is fixed to the bedside or floor. These systems often require large footprint grounding frames which can be undesirable for many clinical applications [18]. Ungrounded bedside robotic controllers transmit force between two ends of a robot, one that is handheld and the other that manipulates tissue. There are several examples of handheld robotic controllers for catheters and endoscopes [19]–[21], however, they use actuators for each DoF in the handle, which increases the mechanical complexity and weight. Our prior work [22], which utilized a motorized 1 DoF bedside controller for a pneumatic soft robot would suffer from similar limitations if scaled to more DoFs.

The stated limitations of current bedside robotic controllers motivate the design and development of a novel controller as depicted in Fig. 1. We use an admittance control framework, in which an input force drives an output motion. In our approach, a 6-DoF force/torque sensor is rigidly attached to a 3D-printed handle on one end and grounded through an adjustable arm mounted to the operating table on the other end. The measured force input is scaled to catheter tip velocity. Although technically a grounded system, it maintains a low footprint as the mounting arm is not motorized. Further, using a force sensor reduces the mechanical complexity and enables simple construction even for several DoFs. Finally, placing the controller at the catheter insertion site allows the operator to easily insert and steer the tip simultaneously.

In this work, we utilize our proposed controller with our previously developed dual-segment fluid-actuated catheter tip, which uses fluidic pressure to individually actuate two serially stacked segments [23]. Applied fluidic pressure [24] is an

This work was supported in part by National Institutes of Health R01EB033354. In addition, the work was supported in part by the Maryland Robotics Center and the Center for Engineering Concepts Development at the University of Maryland. Finally, this material is based upon work supported by the National Science Foundation Graduate Research Fellowship Program under Grant No. DGE 2236417 and 2139757. Any opinions, findings, and conclusions or recommendations expressed in this material are those of the author(s) and do not necessarily reflect the views of the National Science Foundation.

[1]Department of Mechanical Engineering, Johns Hopkins University, Baltimore, MD, USA. Email: {nbarne18, jdelainebrown, axel}@jhu.edu

[2]Laboratory for Computational Sensing and Robotics, Johns Hopkins University, Baltimore, MD, USA. Email: {sjiang44, ldi4}@jhu.edu

[3]Department of Biomedical Engineering, Johns Hopkins University, Baltimore, MD, USA. Email: hqu6@jhu.edu

[4]Department of Diagnostic Radiology and Nuclear Medicine, University of Maryland, Baltimore, Baltimore, MD, USA. Email: miroslaw.janowski@som.umaryland.edu

[5]Children's National Hospital, Department of Pediatrics, George Washington University School of Medicine, Washington, DC, USA. Email: CBerul@childrensnational.org

[6]Department of Mechanical Engineering, University of Maryland, College Park, MD, USA. Email: {acolton1, oyoung, rsochol}@umd.edu

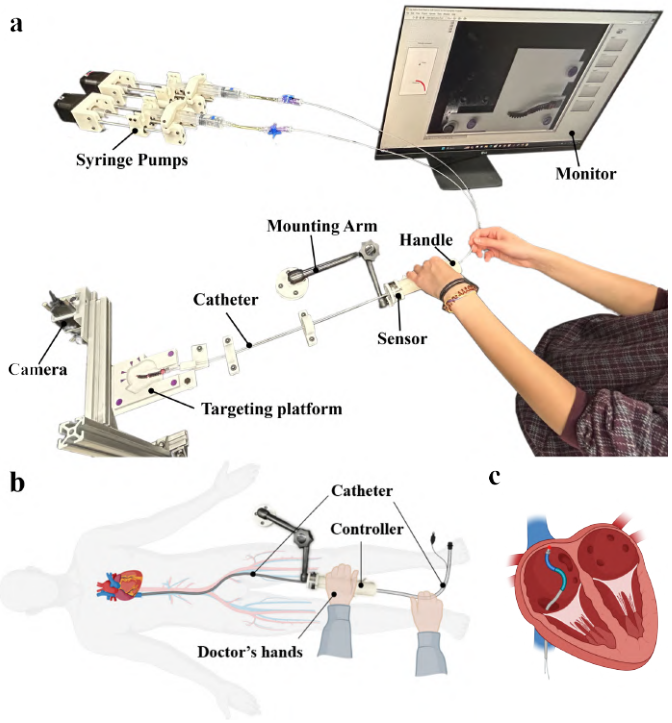

Fig. 1. **a** Experimental platform: the user inserts and retracts the catheter with one hand and simultaneously applies a force to the table-mounted handle with the other hand. **b** The intended configuration of the controller handle in a real procedure, placed at the insertion site to the body. **c** A potential placement of the dual-segmented catheter in the right atrium in the case of cardiovascular intervention. Figure generated with BioRender.

attractive choice of actuation mechanism among others [3], [19], [25] due to its simple control infrastructure and natural compliance, however our control approach is not dependent on this being the actuation mechanism. Further, the use of a dual-segment catheter tip enables better maneuverability than a single segment and is advantageous in a range of procedures [26]–[28]. It also provides a sufficiently complex architecture with which to validate our control approach.

A promising application of a dual-segment soft robotic catheter is cardiac ablation which is used to treat abnormal heart rhythms caused by atrial fibrillation. In this procedure, radiofrequency (RF) energy is emitted from the tip of a catheter to create small, discrete lesions on the cardiac tissue which in turn cause scarring that helps break up the electrical signals that cause irregular heartbeats. During RF ablation, good tip contact with the wall is desirable to minimize the RF power and application time required, therefore minimizing excessive tissue heating [29]. The ability to simultaneously control position and orientation with our robotic catheter could potentially lead to better positioning and contact with the wall relative to standard ablation catheters, which typically have a single bending segment [4]. In this work, we use a planar 3D-printed atrium-like cavity as a test platform to validate the improved targeting accuracy as compared to a baseline task performed by an experienced cardiologist.

To summarize, the contributions of this work are as follows: the design and development of a novel force-sensing bedside control interface for catheter manipulation; the control of a dual-segmented fluidically actuated catheter tip; and the experimental evaluation of the control approach in a simulated ablation task and comparison to the task performed by an experienced cardiologist.

II. Methods

A. Soft Robot Catheter Characterization

The soft robot catheter tip used in this study was fabricated through an additive manufacturing technique with elastic photocurable material. The design, fabrication, and characterization details are described in [23]. The robotic catheter utilizes dual-channel fluidic actuation, provided by two motorized syringe pumps as depicted in Fig. 2a. To characterize the soft robot, water was displaced into the catheter segments via syringe pumps at 0.04 mL/sec, and each segment was cycled (sweeping from maximum to minimum syringe displacement) ten times. Deformation was measured through three pairs of color markers at the base, middle, and tip positions along the length of the catheter tip (see Fig. 2a). We can define the positions of the average of the centroids of each marker in a pair, p_1, p_2, p_3, as well as the direction given by a line through the pair of centroids, n_1, n_2, n_3. Then, the angle and arc length of a single segment are given by:

$$\theta_i = \text{atan2}(n_{i+1,y}, n_{i+1,x}) - \text{atan2}(n_{i,y}, n_{i,x}) \quad (1)$$

$$l_i = \frac{||p_{i+1} - p_i||\theta_i}{2\sin(\theta_i/2)} \quad (2)$$

Where $n_{i,x}$ and $n_{i,y}$ refer to the $x-$ and $y-$components of n_i, and $i \in 1, 2$ is the segment. Images were acquired with a Basler ace 2 USB3 area scan camera (Basler, Germany), with precision of approximately ± 4.5 degrees and ± 0.2 mm in angle and length respectively using the color markers. The segment angles and lengths were fitted to linear functions of syringe displacement which was used for control. The fits had R^2 values of 0.98 and 0.93 for segment 1's angle and length respectively, and values of 0.92 and 0.91 for segment 2's angle and length respectively.

B. Force-Sensing Control Handle

The controller (see Fig. 1a) consists of a 3D-printed handle mounted on a mini40 6-axis force/torque sensor (ATI, United States), which is in turn mounted on an adjustable positioning arm (Noga, Israel) fixed to the table. The mounting arm allows the handle to be placed arbitrarily within the workspace of the arm, and tightening the arm allows for rigid grounding of the sensor. Thus, the handle can be easily placed at the optimal position and angle relative to the anatomy, which is necessary for catheter-based interventions [30]. Further, the force sensor and handle have a hole along their cylinder's axis used for passing the catheter. Thus, the controller increases catheter dexterity without increasing the complexity of the user's movements.

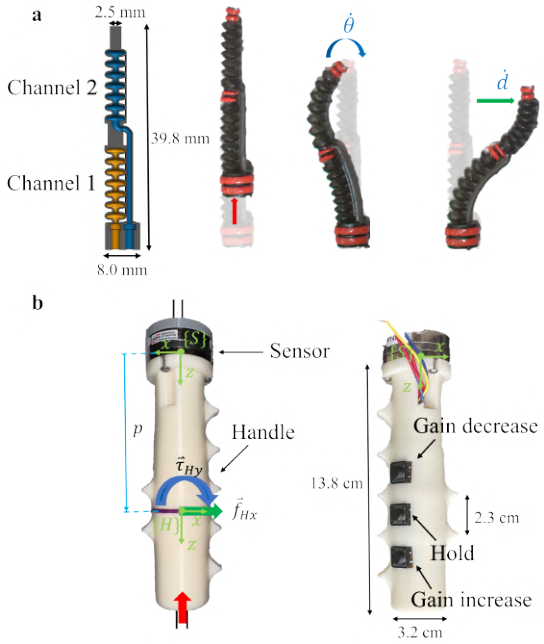

Fig. 2. **a** Dual-segment catheter tip design and movements. The blue fluidic channel and orange fluidic channel can be pressurized independently. The movements can be represented by three DoFs: tip vertical translation (red arrow), tip rotation (blue arc), and tip horizontal translation (green arrow) **b** The movements in (a) are controlled by manual insertion, linear force, and torque about the defined handle frame H which is offset from the sensing frame S by a distance of p. On the other side of the controller, the top and bottom buttons change the gain that scales the force into a desired velocity, and the hold button is pressed to switch between on and off states.

Dual-segment soft actuators have been parameterized in several ways, most often by the angles of each segment [26] or the robot's tip pose [31]. Since our task requires accurate positioning and orienting of the robot's tip, we use tip pose control. In our framework, the user is still required to manually insert the catheter, so we use the two robot fluidic channels to drive the tip angle (θ) and horizontal displacement (d) (Fig 2). The forces exerted by the user's hand are translated into desired velocities as shown in Fig. 2a and b. Velocity control is a natural choice for this interface as the handle is in a fixed position to allow reliable force transmission to the sensor as well as to allow the catheter to be passed through the center without bending it. The homogeneous transformation from the sensing frame S to the handle frame H is given by $g_{S\to H} \in \mathbb{SE}(3)$. Therefore, the force $F_H \in \mathbb{R}^6$ applied in the handle frame is related to the force $F_S \in \mathbb{R}^6$ measured in the sensing frame via:

$$F_H = Ad(g_{S\to H})^T F_S \tag{3}$$

Where $Ad(g) \in \mathbb{R}^{6x6}$ represents the adjoint of rigid body transformation g, and a generalized force is defined as $F = \begin{bmatrix} f_x & f_y & f_z & \tau_x & \tau_y & \tau_z \end{bmatrix}^T$. Given F_H and gains k_d and k_θ, we define the desired tip velocity by a simple force scaling:

$$v_{des} = \begin{bmatrix} \dot{d} \\ \dot{\theta} \end{bmatrix} = \begin{bmatrix} k_d f_{Hx} \\ k_\theta \tau_{Hy} \end{bmatrix} \tag{4}$$

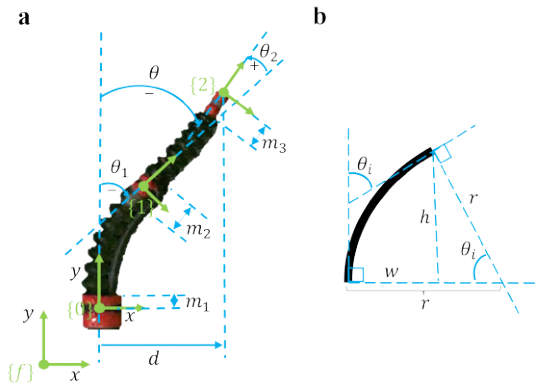

Fig. 3. **a** Kinematic description of the soft robot. Right-handed coordinate systems are placed at the along the length with the y-axis direction defined by the line through the centroids of a given pair of markers and the z-axis coming out of the page **b** The piecewise constant curvature parametrization for a single segment.

As this approach relies on the user implicitly applying F_H about the defined origin of the handle, this origin is marked by a circle and a line along its x-axis. In addition, finger grooves on the handle allow repeatable hand placement. A linear force can be applied by pushing the middle finger or thumb along the painted line and a torque can be applied by rolling the thumb to one side of the groove and pushing the index, ring, and/or little finger. The sizing of the handle and finger grooves are based on median hand sizes [32], [33]. Finally, the buttons depicted in Fig. 2b are placed just beyond the finger grooves such that the fingers can naturally reach them when holding the handle. The gain increase and decrease buttons allow adjustment of the force scaling law in discrete increments. The hold button is used to engage/disengage robotic actuators. When disengaged, the force inputs to the handle are ignored.

C. Constant Curvature Control

Often, continuum robots are conveniently modeled as piecewise constant curves [34], in which each segment is assumed to be a perfectly circular arc. Our robotic catheter is thus assumed to be two circular arcs with straight sections connecting them. The relevant variables labeled in Fig. 3b lead us to the following derivation of the tip position of a single segment relative to the base:

$$\begin{bmatrix} w_i \\ h_i \end{bmatrix} = \begin{bmatrix} -\frac{l_i}{\theta_i}(1-\cos\theta_i) \\ \frac{l_i}{\theta_i}\sin\theta_i \end{bmatrix} \tag{5}$$

Where l_i is the length of the segment. It follows that the rigid transformation from the base to tip of a single constant curvature arc is as follows:

$$g_{a,i} = \begin{bmatrix} R_z(\theta_i) & \begin{bmatrix} w_i \\ h_i \end{bmatrix} \\ 0 & 1 \end{bmatrix} \tag{6}$$

Where $R_z(\theta_i)$ is the two-dimensional in-plane rotation by θ_i. In addition, the transformation from the base to tip of a single straight section is given by:

$$g_{s,i} = \begin{bmatrix} I & \begin{bmatrix} 0 \\ m_i \end{bmatrix} \\ 0 & 1 \end{bmatrix} \tag{7}$$

As such, we can define a rigid transformation between the robot catheter's base frame 0 and the tip frame 2 as follows:

$$g_{0\to 2} = g_{s,1} * g_{a,1} * g_{s,2} * g_{a,2} * g_{s,3} \tag{8}$$

Further, the workspace variables are given by:

$$x = \begin{bmatrix} d \\ \theta \end{bmatrix} = \begin{bmatrix} g_{0\to 2}[1,3] \\ \text{atan2}(g_{0\to 2}[2,1], g_{0\to 2}[1,1]) \end{bmatrix} \tag{9}$$

Where $g[i,j]$ represents the element of g in the i^{th} row and j^{th} column. We can also define an intermediate vector $\tilde{\theta} = \begin{bmatrix} \theta_1 & \theta_2 & l_1 & l_2 \end{bmatrix}^T$ such that $x = f(\tilde{\theta})$. Differentiating gives our system Jacobian J:

$$\frac{\partial x}{\partial t} = \frac{\partial f}{\partial \tilde{\theta}} \frac{\partial \tilde{\theta}}{\partial q} \frac{\partial q}{\partial t} = J \frac{\partial q}{\partial t} \tag{10}$$

Where $q = \begin{bmatrix} q_1 & q_2 \end{bmatrix}^T$ are the syringe pump displacements and t is time. The Jacobian J is then obtained by differentiating equation 9 as well as the relations from segment angle and length to syringe displacement. Due to the linearity of the segment angle and length models, J will only have dependence on $\tilde{\theta}$, which can be obtained in real time using the color markers (equations 1, 2). In practice, we can use the inverse Jacobian in a simple resolved rate controller:

$$\Delta q_{des} = J^{-1} \Delta x_{des} \tag{11}$$

Where $\Delta x_{des} = v_{des} \Delta t$ given v_{des} from equation 4 and timestep Δt. The central controller is implemented on a National Instruments PCIe-6353 data acquisition (DAQ) card (National Instruments, United States) and PC. The DAQ card acquires signals from the force sensor and generates driving signals for the stepper motors in each syringe pump. The closed-loop controller was developed in LabVIEW (National Instruments, United States) and runs at 70 Hz.

III. Experiments and Results

A. System Characterization

The key to intuitive velocity control of the soft robotic catheter is the ability to control each DoF individually and simultaneously, when needed. Thus it is important to characterize the crosstalk between these DoFs to ensure that the user can adequately create a mental mapping of their intended movement to robot motion. Given two channels a and b with values u_a and u_b, the crosstalk percentage c_a in channel a when channel b is being driven is here defined as:

$$c_a = \frac{u_a - u_{a,des}}{u_{a,max} - u_{a,min}} * 100 \tag{12}$$

Where $u_{a,des}$ is the desired constant value of channel a, and $u_{a,max}$ and $u_{a,min}$ are the maximum and minimum values of channel a, respectively. In other words, the crosstalk for a given DoF is expressed as a percentage of its full range. The full ranges for our dual-segment catheter and force/torque controller are as follows: $d \in [-20, 40]$ mm, $\theta \in [-100, 50]$ deg., $f_{Hx} \in [-3.5, 3.5]$ N, and $\tau_{Hy} \in [-0.3, 0.3]$ N-m. A small degree of crosstalk is expected and acceptable, but a high degree of crosstalk may make the operation too difficult.

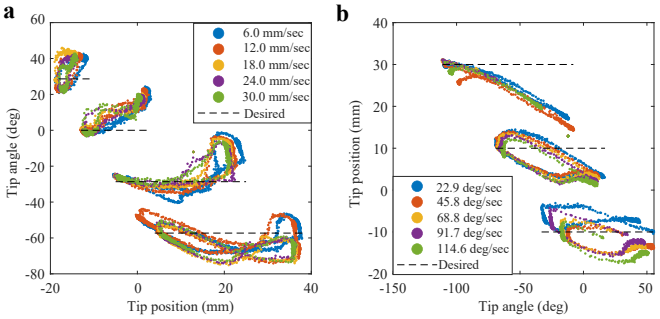

Fig. 4. **a** Attempting to hold tip angle constant while sweeping through the workspace in tip position. **b** Attempting to hold tip position constant while sweeping through the workspace in tip angle.

To characterize follower-side crosstalk, a desired tip angle was defined and the robotic catheter was positioned at that angle and the leftmost tip position in the workspace. Then, a constant linear velocity was commanded until the robot reached the rightmost tip position in the workspace, and then the robot was commanded to return at the same linear velocity. This process was repeated for several velocities and starting tip angles. The whole procedure was then repeated by holding tip positions constant and sweeping through tip angles. The results are depicted in Fig. 4. The maximum position crosstalk is 27% while driving tip angle, and the maximum angle crosstalk is 19% while driving tip position.

To investigate the leader-side crosstalk, a training task was performed to teach four novice users how to apply forces and torques as well as collect data on how well they are able to distinguish forces from torques. After being instructed on hand placement, the users were shown the interface in Fig 5a. The task was to apply the instructed forces and torques such that the red meter representing the measured value reached the black line representing the target. An alternating sequence of forces and torques up to ± 3.5 N and ± 0.3 N-m, respectively, was instructed twice. Either the force or torque was instructed to be a nonzero value at any given trial, not both. Fig. 6 depicts the force crosstalk when driving torque (Fig. 6a) and the torque crosstalk when driving force (Fig. 6b).

The maximum torque crosstalk is 11% when applying a pure linear force and the maximum force crosstalk is 15% when applying a pure torque, thus it was slightly easier for users to exert a pure linear force than a torque. Further, there doesn't seem to be a consistent trend amongst users, however novice 2 exhibited a downward trend in both the pure force and pure torque cases. Overall, the leader side crosstalk is less than that on the follower side.

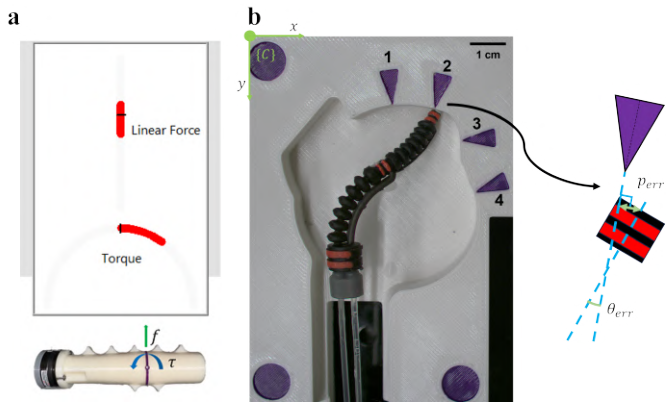

Fig. 5. **a** First, the user is trained on how to use the handle. The image instructs about which point to apply the forces and several target forces are shown as black lines on the meters above for the users to hit. **b** The user then performs the experimental task and errors are calculated as shown.

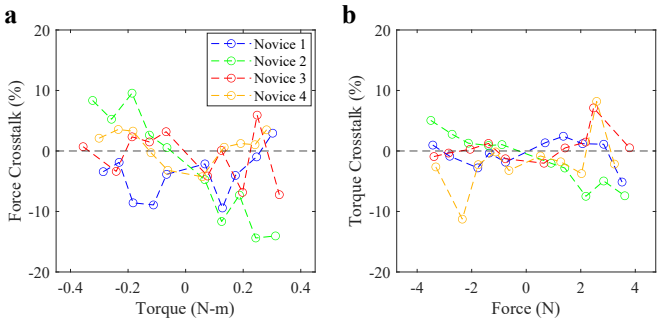

Fig. 6. **a** The force crosstalk percentage when a user is intending to exert a pure torque. **b** The torque crosstalk when a user is intending to exert a pure linear force.

B. Targeting Task Setup

To simulate an ablation-related task with our two-dimensional system, we 3D-printed an atrium-like cavity with four triangular targets placed along the wall as shown in Fig. 5b. The cavity has an approximate diameter of 4.5 cm based on typical right atrium apico-basal diameters [35]. The catheter enters through a vessel analogous to the inferior vena cava (IVC) of diameter 2.0 cm given typical IVC diameters [36]. At the beginning of each trial, the experimenter manually annotates target positions and angles.

The same four novice users from the crosstalk analysis as well as one expert user participated in the study. The novice users had never used the controller or performed the task but they are robotics researchers. The expert is an experienced cardiologist who regularly performs cardiac ablation procedures. A sequence of 40 targets was generated, such that each target appeared ten times. The users were instructed to advance the catheter and steer it to be positioned at and aligned with the targets in the task. The robotic and standard catheters have different stiffness and thus different wall interactions, so only the distance normal to the target line

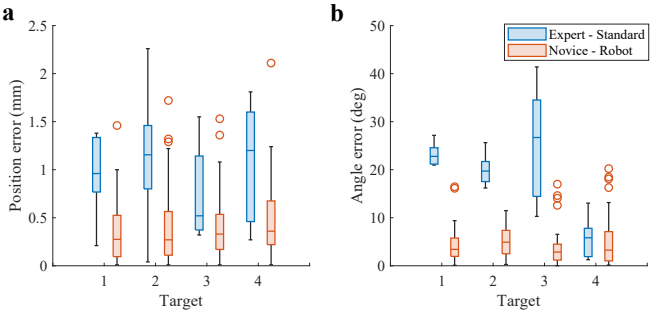

Fig. 7. **a** Distribution of position errors for each target. **b** Distribution of angular errors for each target.

from the target to the catheter tip is recorded as the error. The catheter tip pose was manually annotated on each target image. The total measurement error was ± 0.20 mm and ± 0.37 deg., corresponding to the maximum deviations from the average error across five annotations of the same image. The novice users performed the trials using the soft robot catheter and a standard ablation catheter, while the expert used only the standard catheter to provide a baseline. The ablation catheter used was a bi-directional 8F FlexAbility Ablation Catheter (St. Jude Medical, United States) with an F-J distal curve shape. It was observed that while using the standard catheter, novice users employed the unexpected strategy of digging into the wall with the tip and pivoting around a point on the wall to change the angle. The expert did not employ this strategy, and the strategy is not applicable to the robotic catheter due to the tip's compliance. Further, as this method carries the risk of applying dangerous forces to the tissue and is mostly possible due to the rigidity of the cavity wall, the data is mentioned but not presented visually with the main results (see Fig. 7) since it is not a relevant comparison.

C. Targeting Task Results

The experimental results from the targeting task are shown in Fig. 7. We see that the median is lower for the novice robotic catheter trials than the expert baseline in both position and angle for all targets. Further, the novices using the robotic catheter had position error (mean±SD) of 0.4 ± 0.4 mm and angle error of 4.6 ± 4.2 deg while the expert user had position error of 1.0 ± 0.5 mm and angle error of 18.2 ± 9.6 deg. Using the standard catheter, the novice users achieved a position error of 0.5 ± 0.5 mm and angle error of 8.9 ± 8.7 deg., which was better than the expert's performance due to the unique strategy they employed, however still not as good as the novices' performance with the robotic catheter.

In light of the novice users attaining better targeting accuracy than the expert, it should be noted that the expert user performed their trials in about half the time - 6.1 ± 2.2 s in comparison to 13.6 ± 7.7 s for the novices with the robotic catheter. The improvement in performance for the robotic catheter is not only due to taking a longer time, however, as

with the standard catheter the novice users took about as long (12.2 ± 8.8 s).

In addition, despite each robotic catheter bar in Fig. 7 being composed of 40 trials and the expert's composed of 10 trials, the expert has a similar or larger spread in almost all cases. This indicates that overall, the novices were able to place the robotic catheter more consistently. Interestingly, the expert had angle accuracy on par with the novices on target four. This intuitively makes sense, as looking at Fig. 5b, target four seems the easiest to match the angle of given a single segment catheter, as it approximately lies on and is normal to a circle centered at the entrance to the cavity.

IV. Discussion and Conclusion

There are a few limitations to the study that could alter the ease of use unevenly between the two catheters in comparison to a real intervention. The evaluation takes place in a static, rigid two-dimensional platform with no procedural time limit. However, in clinical scenarios, heart dynamics and the incentive to minimize procedural time likely influence performance. For example, the standard catheter tip is stiffer than our soft robot, improving stability in dynamic environments. The evaluation is also limited in that the path to the heart in a patient's body is more tortuous than the straight path used here (see Fig. 1a). Further, participants could potentially see the catheter tip directly in the platform as well as on the monitor, whereas in a real case the surgeon only has a monitor or virtual view. Lastly, during the novice users' trials, there was frame rate lag which made it more frustrating for the user to visually track the catheter, leading to worse performance.

Despite these limitations, the study presented here serves as a preliminary evaluation that demonstrates the potential utility of the catheter and control system. Users were able to control tip position and orientation effectively, despite some level of crosstalk between DoFs on the leader and follower sides. Thus, the user is able to take advantage of the added dexterity using a simple, easy-to-learn interface. This work adds to the body of research of dual-segment fluidic soft robot parametrization and control [26]–[28], [31], and advances the field by proposing and testing a novel controller that accounts for the requirements of the clinical setting. Although cardiac ablation is our test case, the approach has been applied to a wide range of catheter-based interventions in which precise placement or pointing is required.

In the future, this work can be further improved to increase its clinical relevance. Disposable sleeves and drapes will be used to maintain sterility of the bedside controller for future clinical translation. The ergonomics of the controller can be explored in depth to achieve optimized comfort and force transmission. The catheter tip can be optimized in size, stiffness, and design, to enable its use for a specific procedure. For cardiac ablation, the presented soft robot requires miniaturization from its maximum 8.0 mm diameter to around the 2.7mm diameter of the standard catheter used here. Using our recently reported "ex situ Direct Laser Writing" 3D microprinting strategies [37]–[40], the catheter tip can be fabricated with submillimeter outer diameters (e.g., Fig. 8) to facilitate wide-ranging endovascular interventions. Also, more DoFs should be added to the soft robot to enable steering in three dimensional space. Finally, the control performance can be improved by taking a more sophisticated approach such as developing a more accurate model [41] or using image guidance to estimate a model [42] and a more clinically relevant feedback modality should be used such as intra-operative CT, MRI, electromagnetic tracking, or ultrasound [43].

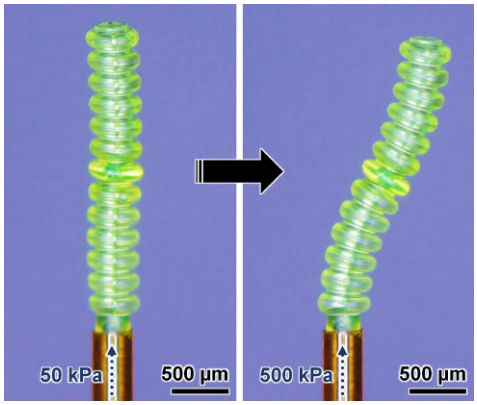

Fig. 8. Experimental results for a 3D-microprinted 1.1 Fr dual-segment soft robotic catheter tip under varying pneumatic pressure.

In summary, we have presented a novel bedside admittance controller for a dual-segment soft robot that improves the positioning and orienting accuracy relative to the baseline. This result indicates that this system has the potential to add precision to catheter-based interventions, enabling higher success rates and better patient outcomes.

References

[1] L. Cruddas, G. Martin, and C. Riga, "Robotic endovascular surgery: current and future practice," *Seminars in Vascular Surgery*, vol. 34, no. 4, pp. 233–240, 2021.

[2] X. Hu, A. Chen, Y. Luo, C. Zhang, and E. Zhang, "Steerable catheters for minimally invasive surgery: a review and future directions," *Computer Assisted Surgery*, vol. 23, no. 1, pp. 21–41, 2018.

[3] T. Soyama, D. Yoshida, Y. Sakuhara, R. Morita, D. Abo, and K. Kudo, "The steerable microcatheter: A new device for selective catheterisation," *CardioVascular and Interventional Radiology*, vol. 40, no. 6, pp. 947–952.

[4] L. M. Haegeli and H. Calkins, "Catheter ablation of atrial fibrillation: an update," *European heart journal*, vol. 35, no. 36, pp. 2454–2459, 2014.

[5] C. C. Nguyen, T. Teh, M. T. Thai, P. T. Phan, T. T. Hoang, J. Davies, H.-P. Phan, C. H. Wang, N. H. Lovell, and T. Nho Do, "A handheld hydraulic soft robotic device with bidirectional bending end-effector for minimally invasive surgery," *IEEE Transactions on Medical Robotics and Bionics*, vol. 5, no. 3, pp. 590–601, 2023.

[6] A. A. Khokhar, A. Zelias, A. Zlahoda-Huzior, and D. Dudek, "Complication during robotic-pci: Iatrogenic guiding catheter dissection," *Catheterization and Cardiovascular Interventions*, vol. 99, no. 5, pp. 1526–1528, 2022.

[7] F. Chen, H. Shen, C. Wang, L. Xie, S. Zhou, and H. Wang, "The model experimental evaluation of the cardiovascular interventional surgery robot system," in *2018 IEEE 16th Intl Conf on Dependable, Autonomic and Secure Computing, 16th Intl Conf on Pervasive Intelligence and Computing, 4th Intl Conf on Big Data Intelligence and Computing and Cyber Science and Technology Congress(DASC/PiCom/DataCom/CyberSciTech)*, 2018, pp. 114–120.

[8] X. Wang, K.-H. Lee, D. K. C. Fu, Z. Dong, K. Wang, G. Fang, S.-L. Lee, A. P. W. Lee, and K.-W. Kwok, "Experimental validation of robot-assisted cardiovascular catheterization: model-based versus model-free control," *International journal of computer assisted radiology and surgery*, vol. 13, p. 797–804, April 2018.

[9] M. A. Tavallaei, M. K. Lavdas, D. Gelman, and M. Drangova, "Magnetic resonance imaging compatible remote catheter navigation system with 3 degrees of freedom," *International Journal of Computer Assisted Radiology and Surgery*, vol. 11, no. 8, pp. 1537–1545, 2016.

[10] N. K. Sankaran, P. Chembrammel, A. Siddiqui, K. Snyder, and T. Kesavadas, "Design and development of surgeon augmented endovascular robotic system," *IEEE Transactions on Biomedical Engineering*, vol. 65, no. 11, pp. 2483–2493, 2018.

[11] W. Peng, Z. Wang, H. Xie, and L. Gu, "Design, development and evaluation of an ergonomically designed dual-use mechanism for robot-assisted cardiovascular intervention," *International journal of computer assisted radiology and surgery*, vol. 18, no. 2, p. 205—216, February 2023.

[12] Z. A. Shaikh, M. F. Eilenberg, and T. J. Cohen, "The amigo remote catheter system: From concept to bedside," *The Journal of innovations in cardiac rhythm management*, vol. 8, no. 8, p. 2795–2802, August 2017.

[13] Y. Zhao, Z. Mei, X. Luo, J. Mao, Q. Zhao, G. Liu, and D. Wu, "Remote vascular interventional surgery robotics: a literature review," *Quantitative Imaging in Medicine and Surgery*, vol. 12, no. 4, pp. 2552–2574.

[14] A. Szold and N. Warnaar, "Robotized mis instruments: Filling the gap between rigid tools and large robotic systems," in *Innovative Endoscopic and Surgical Technology in the GI Tract*, S. Horgan and K.-H. Fuchs, Eds. Springer International Publishing, 2021.

[15] A. Üneri, M. A. Balicki, J. Handa, P. Gehlbach, R. H. Taylor, and I. Iordachita, "New steady-hand eye robot with micro-force sensing for vitreoretinal surgery," in *2010 3rd IEEE RAS & EMBS International Conference on Biomedical Robotics and Biomechatronics*, 2010, pp. 814–819.

[16] J. A. Sánchez-Margallo and F. M. Sánchez-Margallo, "Initial experience using a robotic-driven laparoscopic needle holder with ergonomic handle: assessment of surgeons' task performance and ergonomics," *International journal of computer assisted radiology and surgery*, vol. 12, pp. 2069–2077, 2017.

[17] S. Yang, R. A. MacLachlan, and C. N. Riviere, "Manipulator design and operation of a six-degree-of-freedom handheld tremor-canceling microsurgical instrument," *IEEE/ASME Transactions on Mechatronics*, vol. 20, no. 2, pp. 761–772, 2015.

[18] C. J. Payne, K. Vyas, D. Bautista-Salinas, D. Zhang, H. J. Marcus, and G.-Z. Yang, *Shared-Control Robots*. New York, NY: Springer US, 2021, pp. 63–79.

[19] C. Girerd and T. K. Morimoto, "Design and control of a hand-held concentric tube robot for minimally invasive surgery," *IEEE Transactions on Robotics*, vol. 37, no. 4, pp. 1022–1038, 2021.

[20] L. Xue, X. Yang, C. Zhang, S. Song, and J. Wang, "Ergonomics-based design of handheld concentric tube robot," in *2022 IEEE International Conference on Robotics and Biomimetics (ROBIO)*, 2022, pp. 2057–2062.

[21] J. Legrand, A. Javaux, M. Ourak, D. Wenmakers, T. Vercauteren, J. Deprest, S. Ourselin, K. Denis, and E. Vander Poorten, "Handheld active add-on control unit for a cable-driven flexible endoscope," *Frontiers in Robotics and AI*, vol. 6, 2019.

[22] N. Barnes, O. Young, A. Colton, X. Liu, M. Janowski, D. Gandhi, R. Sochol, J. Brown, and A. Krieger, "Toward a novel soft robotic system for minimally invasive interventions," *International Journal of Computer Assisted Radiology and Surgery*, vol. 18, no. 9, pp. 1547–1557, 2023.

[23] S. Jiang, L. Di, N. Barnes, H. Qu, O. Young, J. D. Brown, R. Sochol, and A. Krieger, "One-piece 3d-printed pneumatic catheter: Dual-channel design with integrated robotics control for endovascular interventions," in *The IEEE 7th International Conference on Soft Robotics (RoboSoft 2024)*, 2024, in pres.

[24] T. Gopesh, J. H. Wen, D. Santiago-Dieppa, B. Yan, J. S. Pannell, A. Khalessi, A. Norbash, and J. Friend, "Soft robotic steerable microcatheter for the endovascular treatment of cerebral disorders," *Science Robotics*, vol. 6, no. 57, p. eabf0601, 2021.

[25] Y. Kim, E. Genevriere, P. Harker, J. Choe, M. Balicki, R. W. Regenhardt, J. E. Vranic, A. A. Dmytriw, A. B. Patel, and X. Zhao, "Telerobotic neurovascular interventions with magnetic manipulation," *Science Robotics*, vol. 7, no. 65, 2022.

[26] H. Abidi, G. Gerboni, M. Brancadoro, J. Fras, A. Diodato, M. Cianchetti, H. Wurdemann, K. Althoefer, and A. Menciassi, "Highly dexterous 2-module soft robot for intra-organ navigation in minimally invasive surgery," *The International Journal of Medical Robotics and Computer Assisted Surgery*, vol. 14, no. 1, 2018.

[27] G. Fang, M. C. K. Chow, J. D. L. Ho, Z. He, K. Wang, T. C. Ng, J. K. H. Tsoi, P.-L. Chan, H.-C. Chang, D. T.-M. Chan, Y. hui Liu, F. C. Holsinger, J. Y.-K. Chan, and K.-W. Kwok, "Soft robotic manipulator for intraoperative mri-guided transoral laser microsurgery," *Science Robotics*, vol. 6, no. 57, 2021.

[28] K. Ikuta, Y. Matsuda, D. Yajima, and Y. Ota, "Pressure pulse drive: A control method for the precise bending of hydraulic active catheters," *IEEE/ASME Transactions on Mechatronics*, vol. 17, no. 5, pp. 876–883, 2012.

[29] H. Nakagawa and W. M. Jackman, "The role of contact force in atrial fibrillation ablation," *Journal of atrial fibrillation*, vol. 7, no. 1, 2014.

[30] V. Yaganti, N. Mejevoi, O. Hasan, M. Cohen, and N. Wasty, "Pitfalls associated with the use of current recommendations for fluoroscopy-guided common femoral artery access," *Catheterization and Cardiovascular Interventions*, vol. 81, no. 4, pp. 674–679, 2013.

[31] Q. Zhao, J. Lai, X. Hu, and H. K. Chu, "Dual-segment continuum robot with continuous rotational motion along the deformable backbone," *IEEE/ASME Transactions on Mechatronics*, vol. 27, no. 6, pp. 4994–5004, 2022.

[32] T. M. Greiner, *Hand anthropometry of US army personnel*. US Army Natick Research, Development & Engineering Center Natick, MA, 1991.

[33] S. Pheasant and C. M. Haslegrave, *Bodyspace: Anthropometry, ergonomics and the design of work*. CRC press, 2018.

[34] I. Robert J. Webster and B. A. Jones, "Design and kinematic modeling of constant curvature continuum robots: A review," *The International Journal of Robotics Research*, vol. 29, no. 13, pp. 1661–1683, 2010.

[35] K. Keller, C. Sinning, A. Schulz, C. Jünger, V. H. Schmitt, O. Hahad, T. Zeller, M. Beutel, N. Pfeiffer, K. Strauch *et al.*, "Right atrium size in the general population," *Scientific reports*, vol. 11, no. 1, p. 22523, 2021.

[36] S. Patil, S. Jadhav, N. Shetty, J. Kharge, B. Puttegowda, R. Ramalingam, and M. N. Cholenahally, "Assessment of inferior vena cava diameter by echocardiography in normal indian population: A prospective observational study," *Indian heart journal*, vol. 68, pp. S26–S30, 2016.

[37] R. Acevedo, Z. Wen, I. B. Rosenthal, E. Z. Freeman, M. Restaino, N. Gonzalez, and R. D. Sochol, "3d nanoprinted external microfluidic structures via ex situ direct laser writing," in *2021 IEEE 34th International Conference on Micro Electro Mechanical Systems (MEMS)*, 2021, pp. 10–13.

[38] S. Sarker, A. Colton, Z. Wen, X. Xu, M. Erdi, A. Jones, P. Kofinas, E. Tubaldi, P. Walczak, M. Janowski *et al.*, "3d-printed microinjection needle arrays via a hybrid dlp-direct laser writing strategy," *Advanced materials technologies*, vol. 8, no. 5, p. 2201641, 2023.

[39] A. Colton, D. Fitzgerald, S. Sarker, N. Barnes, D. Gandhi, M. Janowski, J. D. Brown, J. Kanter, L. Olivieri, M. Fuge, A. Krieger, and R. D. Sochol, "Toward "s"-shaped 3d-printed soft robotic guidewires for pediatric patent ductus arteriosus endovascular interventions," in *The IEEE 7th International Conference on Soft Robotics (RoboSoft 2024)*, 2024, in pres.

[40] B. Felix, O. Young, J. Andreou, N. Portwood, K. Barvenik, N. Barnes, C. R. Weiss, C. Bailey, D. Gandhi, M. Janowski, J. D. Brown, E. Tubaldi, M. Fuge, A. Krieger, and R. D. Sochol, "An approach for 3d microprinting soft robotic surgical tools at 1.5 french length scales for endovascular interventions," in *The IEEE 7th International Conference on Soft Robotics (RoboSoft 2024)*, 2024, in pres.

[41] C. D. Santina, R. K. Katzschmann, A. Bicchi, and D. Rus, "Model-based dynamic feedback control of a planar soft robot: trajectory tracking and interaction with the environment," *The International Journal of Robotics Research*, vol. 39, no. 4, pp. 490–513, 2020.

[42] M. C. Yip and D. B. Camarillo, "Model-less feedback control of continuum manipulators in constrained environments," *IEEE Transactions on Robotics*, vol. 30, no. 4, pp. 880–889, 2014.

[43] A. Ramadani, M. Bui, T. Wendler, H. Schunkert, P. Ewert, and N. Navab, "A survey of catheter tracking concepts and methodologies," *Medical Image Analysis*, p. 102584, 2022.